COVID

Article

Characterization of the SARS-CoV-2 Mutation Pattern Generated In Vitro by the Antiviral Action of Lycorine

Silvina Soledad Maidana [1,2,*,†], Sonia Alejandra Romera [1,2,†], Ana Marandino [3], Rocío Lucia Tau [1], Juan Mauel Shammas [1], Yanina Panzera [3] and Ruben Pérez [3,*]

[1] Institute of Virology and Technological Innovations (IVIT), Dr. Nicolas Repetto and De los Reseros, IVIT (INTA-CONICET), Buenos Aires 1686, Argentina; romera.alejandra@inta.gob.ar (S.A.R.); tau.rocio@inta.gob.ar (R.L.T.); shammas.juan@inta.gob.ar (J.M.S.)
[2] Faculty of Agricultural and Veterinary Sciences, Veterinary Research Institute, University of the Salvador, Buenos Aires B1630AHU, Argentina
[3] Evolutionary Genetics Section, Faculty of Sciences, Institute of Biology, University of the Republic, Montevideo 11400, Uruguay; amarandino@fcien.edu.uy (A.M.); ypanzera@fcien.edu.uy (Y.P.)
* Correspondence: maidana.silvina@inta.gob.ar (S.S.M.); rperez@fcien.edu.uy (R.P.)
† These authors contributed equally to this work.

Abstract

SARS-CoV-2 persists worldwide, driving the demand for effective antivirals that inhibit replication and limit the emergence of resistant variants. Lycorine, a non-nucleoside inhibitor of SARS-CoV-2 RNA-dependent RNA polymerase, exhibits antiviral activity without direct mutagenic effects. Here, we examine the occurrence of single-nucleotide variants (SNVs) and insertions/deletions (indels) in SARS-CoV-2 B.1.499 strain during serial passages in Vero cells, comparing lycorine-treated cultures (2.5 and 5 µg/mL) with untreated controls. Whole-genome sequencing was used to assess mutation patterns and frequencies. Lycorine-treated passages displayed greater variant diversity than controls, with fixed mutations mainly affecting non-structural proteins (Nsp3-F1375A, Nsp5-L50F, and Nsp14-G265D) and the envelope protein (E-S6L). A 15-nucleotide deletion in the *spike* gene (QTQTN motif) occurred in both groups but became fixed only in untreated passages, suggesting negative selection under lycorine pressure. Notably, the L50F mutation in Nsp5, previously linked to nirmatrelvir resistance, was found exclusively in lycorine-treated passages. Additionally, a 1-nucleotide deletion in the accessory gene *ORF8*, detected only under lycorine treatment, resulted in a frameshift mutation that added four amino acids, potentially altering the protein's function. Overall, lycorine induces a distinct mutation profile, favoring replication-related variants while suppressing deleterious deletions. These findings suggest potential mechanisms of cross-resistance and highlight the importance of monitoring resistance during clinical use.

Keywords: SARS-CoV-2; lycorine; antiviral; mutation pattern; viral evolution

Academic Editor: Nadine Alvarez

Received: 28 September 2025
Revised: 14 October 2025
Accepted: 21 October 2025
Published: 23 October 2025

Citation: Maidana, S.S.; Romera, S.A.; Marandino, A.; Tau, R.L.; Shammas, J.M.; Panzera, Y.; Pérez, R. Characterization of the SARS-CoV-2 Mutation Pattern Generated In Vitro by the Antiviral Action of Lycorine. *COVID* **2025**, *5*, 181. https://doi.org/10.3390/covid5110181

1. Introduction

Severe acute respiratory syndrome coronavirus 2 (SARS-CoV-2), the etiological agent of COVID-19, was first identified in December 2019 and has since led to millions of infections and deaths worldwide [1,2]. Although vaccination efforts have significantly reduced COVID-19-related deaths, viral replication can persist after infection, leading to the emergence of genetic variants that can evade immune responses [3–5]. Effective antiviral therapies are needed to suppress replication and limit the development of escape variants.

Antiviral drugs for COVID-19, including molnupiravir, nirmatrelvir, and remdesivir, have achieved significant milestones in reducing disease severity, particularly in high-risk populations [6,7]. Each of these drugs targets distinct steps of the viral replication cycle, shaping different evolutionary trajectories.

Molnupiravir, a ribonucleoside analog, acts through lethal mutagenesis, increasing viral diversity during replication and driving error catastrophe [8,9]. Nirmatrelvir, a primary protease inhibitor, blocks polyprotein processing [10], whereas remdesivir targets the RNA-dependent RNA polymerase (RdRp), inducing delayed chain termination [6,11].

Although effective, these antivirals can exert distinct selective pressures that shape viral evolution. Understanding how new compounds interact with these evolutionary mechanisms is crucial for anticipating resistance pathways and informing combination strategies.

Lycorine ($C_{16}H_{17}NO_4$), a natural phenanthrene alkaloid extracted from the bulbs of the traditional Chinese herb *Lycoris radiata* (Amaryllidaceae), has demonstrated potent anti-SARS-CoV-2 activity in vitro at non-cytotoxic concentrations [12] (Figure 1). It inhibits RdRp by binding to the Asp623, Asn691, and Ser759 residues [12,13]. Molecular docking and dynamics simulations suggest that lycorine can bind to the catalytic dyad (Cys145 and His41) of Mpro, potentially disrupting viral replication [14]. Lycorine's broad-spectrum antiviral properties make it a potential treatment for emerging coronavirus infections [13]. Importantly, lycorine is non-mutagenic, which could reduce the risk of generating new variants compared to nucleoside analogs, such as molnupiravir.

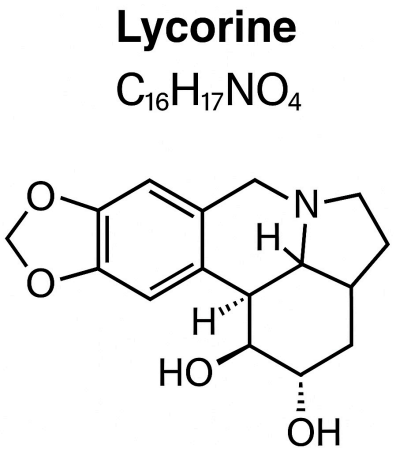

Figure 1. Chemical structure of lycorine ($C_{16}H_{17}NO_4$, PubChem CID 72378).

Despite its promising pharmacological profile, the selective pressures exerted by lycorine on the evolution of SARS-CoV-2 remain unknown. Understanding how antivirals affect viral mutation patterns is crucial for predicting resistance and refining treatment strategies. This study aims to analyze mutation patterns in SARS-CoV-2 under lycorine treatment by conducting in vitro serial passages and comparing viral evolution with and without the drug to identify potential resistance mechanisms.

2. Materials and Methods

2.1. SARS-CoV-2 Isolates and Cell Culture

The SARS-CoV-2 B.1.499 isolate (M07) was used as the initial material for this study. The strain was initially isolated in Buenos Aires, Argentina, in 2020 by the INTA NSBL4 laboratory and was passaged 4 times before storage. An aliquot of this previously isolated and characterized virus stock was provided by the NSBL4 laboratory for experimental purposes. Since no clinical samples or human subjects were collected or handled by our group, ethics committee approval was not necessary. All experimental procedures were conducted in BSL-4 facilities in accordance with institutional biosafety guidelines.

2.2. Antiviral Preparation and Concentration Selection

Vero cells (American Type Culture Collection, Manassas, VA, USA) were maintained in MEM-E medium (Gibco, Thermo Fisher Scientific, Waltham, MA, USA) supplemented with 10% fetal bovine serum (FBS), 100 U/mL penicillin, and 100 μg/mL streptomycin, and incubated at 37 °C in a humidified atmosphere containing 5% CO_2. For antiviral assays, cells were seeded at the appropriate density and used at low passage numbers (<20) to ensure consistent susceptibility to infection.

Lycorine (Sigma-Aldrich, St. Louis, MO, USA) was dissolved in ultrapure water to 25 mg/mL and stored at −20 °C until use.

Cytotoxicity assay (CC_{50} determination): Cytotoxicity was evaluated using the neutral red uptake assay, which measures the ability of viable cells to incorporate and retain the dye. Vero cells were seeded in 96-well plates and incubated for 24 h at 37 °C and 5% CO_2. Twelve concentrations of lycorine (20 to 0.009 μg/mL; twofold serial dilutions) were tested. Each concentration was assayed in triplicate across three independent plates (n = 9 data points per concentration). Untreated cells served as a positive control. After 2 h of drug exposure, the medium was replaced and the cells were incubated for an additional 48 h. Neutral red dye (50 μg/mL final concentration) was then added and incubated for 3 h, followed by dye extraction with a water-ethanol-acetic acid solution (50:49:1). Absorbance was measured at 540 nm using a microplate reader, and the 50% cytotoxic concentration (CC_{50}) was estimated from the dose–response curves by non-linear regression.

Antiviral activity assay (IC_{50} determination): For antiviral testing, Vero cells were infected with SARS-CoV-2 at a multiplicity of infection (MOI) of 0.1 for 45 min at 37 °C and 5% CO_2. The same concentration range used in the cytotoxicity assay was applied in triplicate across three independent plates. After 2 h of drug exposure, the medium was replaced and the cells were incubated for 48 h before neutral red staining and measurement at 540 nm. IC_{50} values were determined from dose–response curves using non-linear regression.

Concentration selection and selectivity index: The selectivity index (SI) was calculated as CC_{50}/IC_{50}. The IC_{50} was determined to be 3.3 ± 0.1 μg/mL, and the CC_{50} was 16 μg/mL. To define working concentrations for subsequent experiments, three concentrations were selected: 2.5 μg/mL (below IC_{50}), 5 μg/mL (close to IC_{80}), and 20 μg/mL (well above CC_{50}), allowing assessment of antiviral activity under suboptimal and inhibitory conditions. All experiments were performed in biosafety level 3 (BSL-3) facilities.

2.3. Serial Passage Protocol

Vero cells were seeded in 6-well plates and infected with SARS-CoV-2 at a multiplicity of infection (MOI) of 0.1 for 45 min at 37 °C.

After infection, the cells were washed twice with phosphate-buffered saline (PBS) and treated with lycorine for 2 h. After treatment, the cells were rinsed again and maintained in MEM-E supplemented with 2% FBS for 72 h. Supernatants were then collected, clarified by centrifugation (3000× g for 10 min), and used for subsequent passages. The cytopathic effect (CPE) was monitored daily. If no CPE was observed, cell lysates were subjected to freeze–thaw cycles before passaging.

No biological replicates were performed, consistent with the exploratory nature of this study. The aim was to characterize the selective landscape induced by lycorine across successive passages of a single viral lineage, providing proof-of-concept data for future confirmatory studies with multiple isolates and replicates.

2.4. Viral Quantification

Viral titers were measured using endpoint titration with serial tenfold dilutions in MEM-E, applied in quadruplicate to Vero cell monolayers in 96-well plates. The plates

were incubated for 45 min at 37 °C, then replaced with MEM-E containing 2% FBS. After 72 h, the cells were checked for cytopathic effects (CPE), and viral titers were calculated using the Reed-Muench method [15].

2.5. RNA Extraction and Whole-Genome Sequencing

Viral RNA was extracted from 200 µL of culture supernatant using the QIAamp Viral RNA/DNA Kit (Qiagen, Hilden, Germany) following the manufacturer's instructions. Whole-genome sequencing was performed using the COVIDSeq assay from Illumina (Illumina Inc., San Diego, CA, USA), which employs a modified version of the ARTIC multiplex PCR [16]. Reverse transcription library preparation was carried out using 8.5 µL of RNA with dual indexing (IDT for Illumina-PCR Indexes Set 3). Whole-genome sequencing was then performed on an Illumina MiniSeq platform using the MiniSeq™ Mid Output Reagent Cartridge (300 cycles, paired-end reads).

2.6. Genome Assembly and Analysis

Sample adapter quality trimming and filtering of raw data were performed using BBDuk in Geneious Prime 2020.1.2 (https://www.geneious.com accessed on 1 December 2024). Clean reads were mapped to the Wuhan reference genome (NC_045512.2) consensus genome to generate the annotated consensus of the first untreated passage. This consensus served as a reference for mapping subsequent passages using Minimap2. Variants (single-nucleotide polymorphisms and indels) with a frequency greater than 5% were annotated in the consensus sequence of each passage. Multiple sequence alignments were generated with MAFFT version 7 [17]. A total of 19 SARS-CoV-2 genomes were analyzed, including 8 passages without antiviral treatment (control: C) and 10 passages with lycorine treatment (antiviral: AV). Variants were classified by frequency: minority (5–50%), major (50–90%), and fixed (>90%). Only variants detected in at least two passages with frequencies above 5% were considered significant, excluding those within primer binding sites.

3. Results

The results describe the antiviral effect of lycorine during serial passages of SARS-CoV-2 in Vero cells, followed by genomic analysis to identify adaptive mutations associated with antiviral pressure.

3.1. In Vitro Antiviral Activity

Lycorine demonstrated concentration-dependent antiviral activity with a selectivity index (SI) of 5.1, an EC_{50} of 16.8 ± 0.1 µg/mL, and an IC_{50} of 3.3 ± 0.1 µg/mL. At the highest concentration (5 µg/mL), viral replication was inhibited entirely by passage 2, with subsequent passages showing a gradual recovery in titer (Table 1). The 2.5 µg/mL concentration allowed for continuous viral propagation while maintaining selective pressure.

Table 1. Viral Titers in Supernatants with and without Antiviral Treatment.

Passage	5 µg/mL	2.5 µg/mL	Untreated
1	10^2	10^3	$10^{6.5}$
2	0	10^2	10^3
3	0	10^5	$10^{5.5}$
4	0	$10^{2.5}$	$10^{3.7}$
5	0	$10^{5.5}$	$10^{5.25}$
6–11	0	10^4–10^6	10^5–$10^{7.25}$

These findings established the working concentrations used for subsequent serial passages and mutation tracking.

3.2. Genome Assembly

Successful whole-genome sequencing yielded 18 high-quality consensus sequences, each 29,862 bp long. This included eight untreated controls (C: 2–5 and 8–11) and nine lycorine-treated passages (AV: 2–10). All samples had coverage depths exceeding 200×, ensuring dependable variant detection. The first consensus sequence from the first untreated sample (passage 1) served as a reference for variant detection and comparative analysis.

The assembled genomes have been deposited in GenBank under BioProject PRJNA1332295, with corresponding BioSample, SRA, and GenBank accessions listed in Supplementary Table S1.

The assembled genomes were then compared to detect and quantify mutations that emerged during serial passages under antiviral pressure.

3.3. Mutation Patterns

To assess the influence of lycorine on SARS-CoV-2 evolution during serial passages, we analyzed single-nucleotide variants (SNVs) and insertions/deletions (indels) across all samples (Table 2, Figure 2). Distinct mutation profiles were observed between lycorine-treated and untreated lineages. Untreated passages accumulated mainly transient minority variants that rarely reached fixation, whereas lycorine-treated lineages displayed increased variant diversity and multiple fixed substitutions.

Table 2. Variant frequencies across cell-culture passages (P).

P	Nsp3 T1319A	Nsp3 F1375A	Nsp5 L50F	Nsp5 L67F	Nsp6 L158I	Nsp12 586 (syn)	Nsp14 G265D	Nsp14 H427Y	Nsp16 199 (syn)	Nsp16 273 (syn)	S T76S	S 15nt Del	S D1259H	E-S6L	*ORF8* 1-nt Del	N-G96N
2-C														13.1		
3-C												8.7	7.3	87.3		
4-C								15.9				16.2	5.8	95.1		
5-C								23.4				55.65		99.4		
8-C											37.2	97.05		100		5.3
9-C									6.8		52.4	97.35	7.3	99.9		
10-C						18.9			18.7		66.2	95.4	7.9	99.9		9
11-C						16.4			10.2		78.5	96.7	6.3	99.7		
1-AV													8.4			
2-AV												9.55				
3-AV	13.1		5.5									33.2	6.9	29.1		
4-AV	18.9	12.8	5.8									36.05	5.4	39.3		
5-AV		26	17.9		42.9		16.1			17.3		67.9	6	20.8	15.1	
6-AV		35.3	25		44.9		25.9			33.3		63.15	6.3	22.3	25.4	5.9
7-AV		87.2	89.5	12.3	7		87.1			93.3		7.95	9.7	88.2	90.9	5
8-AV		92.3	93.6	20			93.5			91		5.95	7.5	92.6	92.6	
9-AV		95.9	96.7	36.1			96.8			97.2			6.6	95.8	95.7	10.3
10-AV		92.5	94.9	34.8			95			86.4		7.05	7.5	99.4	98.3	

3.3.1. Variants in Untreated Passages

Untreated passages showed numerous minority variants (5–50% frequency) that remained transient throughout the experiment. Notable low-frequency variants included a synonymous change at position 586 in the *nsp12* gene, resulting in an H427Y substitution in the Nsp14 protein; a synonymous change at position 199 in Nsp16; the D1259H substitution in the spike (S) protein; and the synonymous N-G96N variant in the nucleocapsid (N) protein. The inconsistent detection of these variants across passages suggests a slight selective advantage under control conditions.

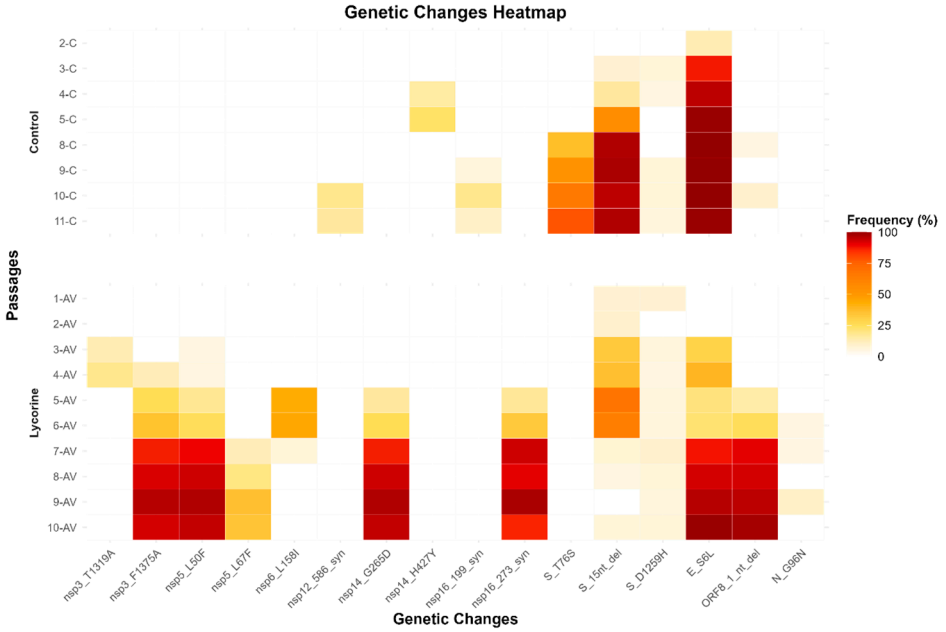

Figure 2. Heatmap displaying the genetic changes in lycorine-treated cell passages (above) and control passages without lycorine (below). Passages with the antiviral exhibit a higher proportion of variants that reach fixation.

In contrast, variants that reached frequencies over 50% followed a notably different pattern. The S-T76S substitution gradually shifted from being rare to becoming fixed by passage 11. A 15-nucleotide deletion in the S gene, which removes the QTQTN motif (amino acids 675–679) near the furin cleavage site, also reached high frequency and eventually became fixed. Additionally, the E-S6L mutation in the envelope protein consistently achieved fixation across untreated passages, indicating a significant selective advantage in the Vero cell culture environment.

3.3.2. Variants in Lycorine-Treated Passages

Under lycorine exposure, a distinct set of mutations emerged. Treated passages displayed higher variant diversity, with several substitutions reaching fixation that were either absent or rare in untreated controls (Figure 2). Other variants reached frequencies below 50%, including Nsp3-T1319A (13.1–18.9%), Nsp5-L67F (12.3–36.1%), Nsp6-L158I (7.0–44.9%), S-D1259H (5.4–9.7%), and N-G96N (5.0–10.3%).

However, by passage 8-AV, several variants had become fixed, including Nsp3-F1375A, Nsp5-L50F, Nsp14-G265D, and a synonymous mutation in Nsp16. Interestingly, the E-S6L mutation—common to both conditions—became fixed later under lycorine treatment, suggesting delayed adaptation dynamics under antiviral pressure.

A unique one-nucleotide deletion in *ORF8* was detected exclusively in lycorine-treated passages. This deletion of a single base (A) occurs at the first position of the last codon, just before the stop codon, shifting the reading frame and producing a new stop codon (TAA) twelve nucleotides downstream. As a result, this deletion leads to a substitution of the last amino acid (Ile → Ser). It extends the protein by four amino acids (Ala, Arg, Thr, Asn), generating a putative 125-amino-acid variant instead of the canonical 121-amino-acid polypeptide. The new stop codon is positioned in the intergenic region preceding the n gene (Figure 2).

The 15-nucleotide *spike* deletion, which became fixed in untreated passages, notably decreased in frequency after passage 6-AV during lycorine treatment, indicating that negative selection pressure from the antiviral acted against this variant (Figure 3).

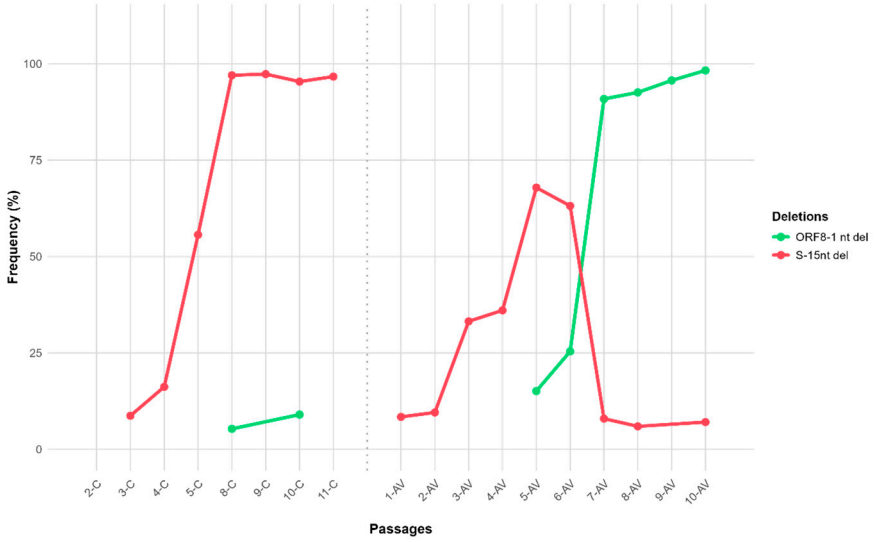

Figure 3. The behavior of deletion variants in passages without lycorine antiviral (**left**) and with lycorine (**right**) is illustrated. The 15-nt deletion became fixed only in passages without lycorine, whereas the 1-nt deletion that resulted in a 4-amino acid insertion emerged and became fixed only in passages with lycorine.

3.4. Comparative Analysis

A comparative analysis of mutation frequencies across passages (Table 2, Figures 2 and 3) revealed two contrasting evolutionary trajectories. In untreated lineages, the spike QTQTN deletion steadily increased and became fixed by the final passage. In contrast, in lycorine-treated passages, this deletion declined sharply after passage 6-AV (<10%) (Figure 3).

Conversely, mutations in non-structural proteins (Nsp3-F1375A, Nsp5-L50F, and Nsp14-G265D) and the ORF8 protein extension progressively increase in lycorine-treated passages, reaching over 90% frequency in the last three passages.

Together, these results demonstrate that lycorine exerts a selective pressure that modifies the trajectory of viral adaptation in vitro, promoting fixation of unique mutations while suppressing variants associated with attenuated phenotypes.

4. Discussion

Understanding how antiviral pressure influences SARS-CoV-2 evolution requires examining not only the specific mutations that arise during treatment but also the broader selective pressures that drive viral adaptation. In this study, we first identify the individual mutations fixed under lycorine treatment and their potential functional impacts on key viral proteins, including components of the replication complex, structural proteins, and accessory factors. We then situate these findings within a broader evolutionary and therapeutic context by comparing lycorine's mutational pattern with those caused by established antivirals such as molnupiravir, remdesivir, and nirmatrelvir.

4.1. Functional Implications of Selected Mutations

4.1.1. Non-Structural Protein Mutations

Mutations in non-structural proteins often have a more direct or significant impact on viral replication and antiviral resistance than changes in structural or accessory proteins, because NSPs frequently perform enzymatic functions essential to replication and drug interactions (e.g., polymerases, proteases, exonucleases). In fact, many known resistance mutations are found in non-structural ORFs rather than structural genes [18].

Nsp3 (T1319A, F1375A): Nsp3 is a multifunctional, multi-domain protein involved in replication complex formation and immune evasion through its papain-like protease

domains [19]. Due to its considerable size and functional diversity, mutations in different regions of Nsp3 can have various effects on viral replication and pathogenesis. Although substitutions in macrodomain 1 can markedly affect replication efficiency [20], residues 1319 and 1375 are outside this region and have not been reported to be variable. The exclusive fixation of F1375A in lycorine-treated passages suggests a possible role in modulating protease activity or compensating for replication deficits under RdRp inhibition, though experimental validation is required.

Nsp5 (L50F, L67F): The *nsp5*-encoded main protease (Mpro/3CLpro) is a homo-dimeric cysteine enzyme that cleaves viral polyproteins, a prerequisite for viral maturation [21]. The L50F substitution, although distant from the catalytic site, is associated with reduced nirmatrelvir susceptibility when combined with active-site mutations such as E166A/V [22–24]. Structural and biochemical studies indicate that L50F can restore enzyme–substrate interactions and rescue the proteolytic activity compromised by these resistance mutations [25].

Nsp14 (G265D): Nsp14 combines a 3′–5′ exonuclease (ExoN) domain, which ensures replication fidelity, and an N7-methyltransferase domain necessary for mRNA capping [26]. The G265D mutation, identified exclusively in lycorine-treated passages, is located within the ExoN domain (residues 1–287) and is predicted to be deleterious [27]. Changes in proofreading efficiency could allow the buildup of specific adaptive mutations or co-evolved mutational sets under selective pressure.

4.1.2. Structural Proteins

Spike QTQTN deletion: In untreated passages, the 15-nt QTQTN deletion adjacent to the furin cleavage site became fixed, but it was suppressed entirely under lycorine treatment (Figure 3). This deletion shortens and rigidifies an external loop adjacent to the furin cleavage site, reducing accessibility to host proteases such as TMPRSS2 (transmembrane serine protease 2), impairing spike processing and attenuating viral replication [28]. Lycorine appears to amplify these replication deficits, further disadvantaging already compromised variants in Vero cells.

Envelope protein (E-S6L): The S6L substitution, fixed under both treated and untreated conditions, likely reflects an adaptation to Vero cells rather than a lycorine-specific effect. Situated in the short N-terminal cytoplasmic domain, it may influence viroporin activity or viral assembly [29,30].

4.1.3. Accessory Proteins

ORF8 frameshift—ORF8 modulates host responses and is dispensable in vitro but can influence infection in vivo [31–33]. Lycorine-treated passages contained a 1-nt deletion causing a frameshift and a C-terminal extension of four amino acids. While deletions in ORF8 often result in a complete loss of function [34–37], this mutation increases its length, potentially affecting stability or host interactions [38].

Together, non-structural, structural, and accessory proteins reveal two distinct evolutionary processes: amino acid substitutions in replication-associated proteins (e.g., Nsp3, Nsp5, Nsp14), which reflect direct adaptive responses to selective pressure, and insertions/deletions (indels) in structural and accessory components (spike, ORF8), which likely result from indirect or compensatory evolutionary dynamics. This combined mutation pattern provides a functional basis for interpreting lycorine's evolutionary impact in the following section.

4.2. Lycorine's Selective Pressure and Mutational Pattern

Building on these mutational insights, we then investigate how lycorine influences the overall evolutionary landscape of SARS-CoV-2 in vitro and how this differs from other antiviral selective regimes.

Our findings show that lycorine, despite not being mutagenic, exerts clear, structured selective pressure on SARS-CoV-2. This pressure drives both an increase in intrapopulation variant diversity and the fixation of specific adaptive mutations, particularly amino acid substitutions in replication-associated genes (*nsp3*, *nsp5*, *nsp14*, and *nsp16*) and an indel event in *ORF8* (Figure 2). At the same time, lycorine suppresses the fixation of deleterious structural changes, such as the QTQTN deletion in the *spike* gene (Figure 3), which commonly emerges and reaches high frequencies in untreated populations. By contrast, control lineages accumulate mostly transient, low-frequency variants without consistent fixation events.

This distinctive mutational pattern under lycorine becomes even more evident when contrasted with the resistance mechanisms induced by currently approved antivirals. Molnupiravir exerts a broad, genome-wide mutagenic effect, increasing intra-host viral diversity without favoring specific adaptive variants [8,9,39]. Experimental evolution studies have shown that SARS-CoV-2 has a high genetic barrier to resistance against molnupiravir, with no consistent resistance-conferring substitutions even after multiple passages [40]. This profile reflects its mechanism of action, based on random nucleotide mispairing and error catastrophe, rather than targeted selection.

In contrast, nirmatrelvir and remdesivir generate focused, target-specific resistance patterns. Nirmatrelvir inhibits the main protease Mpro (Nsp5), blocking viral polyprotein cleavage required for replication. Resistance arises primarily from active-site substitutions (i.e., E166V/A and L167F), often accompanied by compensatory changes like L50F that restore enzymatic activity and viral fitness [25]. Remdesivir, on the other hand, exerts selective pressure on the viral RdRp (Nsp12), with recurrent substitutions including F480L, V557L, and S759A that alter nucleotide discrimination and reshape the polymerase active site, thereby interfering with RDV-TP incorporation [41,42]. Unlike molnupiravir, this directed resistance mechanism involves specific and recurrent substitutions, facilitating molecular surveillance.

The mutation landscape under lycorine, characterized by adaptive changes in Nsp3 (F1375A), Nsp5 (L50F), Nsp14 (G265D), and an ORF8 frameshift, along with the suppression of the spike QTQTN deletion, clearly differs from the pathways observed with nirmatrelvir and remdesivir. Taken together, these patterns highlight three contrasting selective regimes: broad, random mutational pressure (molnupiravir); drive targeted resistance (remdesivir and nirmatrelvir); and multilocus adaptation across functional modules (lycorine).

Notably, the fixation of L50F, a mutation linked to protease inhibitor resistance, suggests that lycorine can select for changes in viral proteins targeted by other drugs, creating a potential cross-resistance interface between therapeutic classes. In parallel, docking analyses indicate that lycorine could interact directly with the catalytic dyad of Mpro (Cys145 and His41), potentially disrupting its protease activity [14]. Although this mechanism remains speculative, it provides a plausible biochemical rationale for the indirect selection of L50F, which may act as a compensatory or stabilizing mutation to maintain enzymatic function under drug pressure. Together, these findings highlight two complementary but distinct pathways through which lycorine may shape Mpro evolution: indirect selection of resistance-associated mutations and potential direct interference with protease activity.

These contrasting evolutionary signatures illustrate how distinct antiviral mechanisms shape SARS-CoV-2 adaptation via predictable yet distinct evolutionary pathways, with clear implications for drug design, resistance monitoring, and therapeutic strategies.

4.3. Clinical, Surveillance, and Development Implications

Our findings have direct implications for both clinical management and genomic surveillance strategies. Resistance monitoring should extend beyond primary drug targets

to include secondary adaptive markers, particularly in scenarios involving combination therapy or prolonged antiviral exposure in immunocompromised hosts. The emergence of the L50F mutation in Mpro (Nsp5) under lycorine pressure exemplifies how antiviral stress can act beyond its primary target, creating a potential cross-resistance interface with protease inhibitors. This underscores the importance of implementing broader molecular surveillance encompassing multiple viral proteins [22–24].

From a therapeutic development perspective, the identification of adaptive mutations in both Nsp5 and Nsp14 highlights the multilayered nature of antiviral resistance. Combining lycorine with compounds that target complementary viral functions, such as RdRp or exonuclease inhibitors, could enhance viral suppression and reduce the likelihood of adaptive escape [43,44]. Moreover, the bottleneck effect observed under lycorine treatment suggests that this compound may be strategically incorporated into combination therapies to restrict viral evolutionary flexibility while preserving antiviral potency.

Integrating lycorine-associated molecular markers, such as L50F and G265D, into SARS-CoV-2 genomic surveillance frameworks could facilitate early detection of adaptive trajectories, particularly in patients with persistent infections. Real-time monitoring of these markers would provide actionable information for individualized clinical decisions and broader public health interventions.

In addition, adjunctive therapeutic interventions, such as compounds with antioxidant or anti-inflammatory properties, could further reduce viral replication and oxidative stress, reducing the risk of cross-resistant variants [45]. Collectively, these results position lycorine as a promising candidate within an integrated antiviral strategy that combines therapeutic innovation with enhanced molecular surveillance. In this context, lycorine-associated mutations may serve not only as molecular markers of antiviral pressure but also as early indicators of emerging resistance networks.

4.4. Study Limitations and Future Directions

This study was performed exclusively with Vero cells, a well-established and commonly used model for propagating SARS-CoV-2 and testing antivirals. These cells support robust viral replication in the absence of exogenous proteases, providing a highly consistent and reproducible system for measuring antiviral activity. Their lack of endogenous type I interferon production reduces variability in host responses, making it easier to compare results across different labs and ensuring consistent evaluation of mutation patterns and drug effects [46–49].

However, the lack of human-specific immune and metabolic pathways limits their ability to accurately model host–virus interactions, especially interferon-mediated responses and drug metabolism. Therefore, the mutation patterns and selective pressures observed should be interpreted within the context of this simplified in vitro system.

Moreover, the suboptimal lycorine concentrations required to sustain viral replication may have introduced artificial selective pressures distinct from those expected under therapeutic exposure levels. Future research should employ physiologically relevant concentration ranges and extend the analysis to primary human airway epithelial cultures, organoid systems, or suitable animal models to validate whether the selective effects observed persist under more realistic biological conditions.

Clinical studies evaluating lycorine's efficacy, safety, and resistance potential across diverse patient populations will be crucial in determining its translational relevance. Additionally, the structural and functional characterization of the identified mutations will be essential for understanding their roles in viral fitness and the antiviral response.

5. Conclusions

Lycorine exerts a selective bottleneck in SARS-CoV-2 populations, increasing variant diversity while promoting the fixation of specific adaptive mutations in non-structural and accessory proteins, and simultaneously suppressing deleterious spike deletions. The fixation of the protease mutation L50F, previously associated with nirmatrelvir resistance, demonstrates that selective pressure can extend beyond a drug's primary target, potentially affecting the effectiveness of other antiviral classes. This finding highlights the risk of cross-resistance and underscores the need to expand genomic surveillance to include not only primary drug targets but also secondary adaptive markers. The early detection of such mutations could provide critical insights into emerging evolutionary pathways that may compromise treatment effectiveness.

More broadly, these results support the strategic combination of lycorine with other antivirals and the implementation of comprehensive resistance monitoring programs. Ultimately, this study illustrates how antiviral pressure actively shapes viral evolutionary trajectories, with tangible consequences for therapeutic efficacy and epidemiological dynamics.

Supplementary Materials: The following supporting information can be downloaded at: https://www.mdpi.com/article/10.3390/covid5110181/s1. Supplementary Table S1. SARS-CoV-2 sequencing data with BioSample; SRA; and GenBank accessions (BioProject PRJNA1332295).

Author Contributions: Conceptualization, S.S.M. and S.A.R.; data curation, R.P.; formal analysis, R.L.T., Y.P. and A.M.; methodology, S.S.M., A.M., J.M.S. and Y.P.; project administration and supervision, S.S.M. and S.A.R.; writing—original draft, S.S.M. and R.P.; resources, S.S.M. and S.A.R.; writing—review and editing, R.P. and S.S.M. All authors have read and agreed to the published version of the manuscript.

Funding: This research was partially funded by Research, Development, and Innovation projects funded by the ArgenINTA Foundation, Castelar Delegation, 2021/22.

Data Availability Statement: The sequencing data generated in this study have been deposited in the NCBI databases under BioProject PRJNA1332295. The corresponding BioSample, SRA, and GenBank accession numbers for each isolate are provided in Supplementary Table S1. Briefly, raw sequencing reads are available in the Sequence Read Archive (SRA), while assembled genomes have been deposited in GenBank under the following accessions: PX397336–PX397353, together with the reference sequence PX397335. This dataset includes both control passages (2-C, 3-C, 4-C, 5-C, 8-C, 9-C, 10-C, 11-C) and antiviral-treated passages (1-AV through 10-AV).

Acknowledgments: The authors would like to thank the NSBL4 laboratory at INTA for its technical assistance and for providing the initial viral isolate.

Conflicts of Interest: The authors declare no conflicts of interest related to this research.

References

1. Chung, Y.-S.; Lam, C.-Y.; Tan, P.-H.; Tsang, H.-F.; Wong, S.-C.C. Comprehensive Review of COVID-19: Epidemiology, Pathogenesis, Advancement in Diagnostic and Detection Techniques, and Post-Pandemic Treatment Strategies. *Int. J. Mol. Sci.* **2024**, *25*, 8155. [CrossRef]
2. Kumar, A.; Sharma, A.; Tirpude, N.V.; Thakur, S.; Kumar, S. Combating the Progression of Novel Coronavirus SARS-CoV-2 Infectious Disease: Current State and Future Prospects in Molecular Diagnostics and Drug Discovery. *CMM* **2023**, *23*, 127–146. [CrossRef]
3. Carabelli, A.M.; Peacock, T.P.; Thorne, L.G.; Harvey, W.T.; Hughes, J.; COVID-19 Genomics UK Consortium; Peacock, S.J.; Barclay, W.S.; de Silva, T.I.; Towers, G.J.; et al. SARS-CoV-2 Variant Biology: Immune Escape, Transmission and Fitness. *Nat. Rev. Microbiol.* **2023**, *21*, 162–177. [CrossRef]
4. Chakraborty, C.; Sharma, A.R.; Bhattacharya, M.; Lee, S.-S. A Detailed Overview of Immune Escape, Antibody Escape, Partial Vaccine Escape of SARS-CoV-2 and Their Emerging Variants with Escape Mutations. *Front. Immunol.* **2022**, *13*, 801522. [CrossRef]

5. Jena, D.; Ghosh, A.; Jha, A.; Prasad, P.; Raghav, S.K. Impact of Vaccination on SARS-CoV-2 Evolution and Immune Escape Variants. *Vaccine* **2024**, *42*, 126153. [CrossRef]
6. Aiello, T.F.; García-Vidal, C.; Soriano, A. Antiviral Drugs Against SARS-CoV-2. *Rev. Esp. Quimioter.* **2022**, *35*, 10–15. [CrossRef] [PubMed]
7. Jayk Bernal, A.; Gomes Da Silva, M.M.; Musungaie, D.B.; Kovalchuk, E.; Gonzalez, A.; Delos Reyes, V.; Martín-Quirós, A.; Caraco, Y.; Williams-Diaz, A.; Brown, M.L.; et al. Molnupiravir for Oral Treatment of COVID-19 in Nonhospitalized Patients. *N. Engl. J. Med.* **2022**, *386*, 509–520. [CrossRef] [PubMed]
8. Maas, B.M.; Strizki, J.; Miller, R.R.; Kumar, S.; Brown, M.; Johnson, M.G.; Cheng, M.; De Anda, C.; Rizk, M.L.; Stone, J.A. Molnupiravir: Mechanism of Action, Clinical, and Translational Science. *Clin. Transl. Sci.* **2024**, *17*, e13732. [CrossRef] [PubMed]
9. Teli, D.; Balar, P.; Patel, K.; Sharma, A.; Chavda, V.; Vora, L. Molnupiravir: A Versatile Prodrug Against SARS-CoV-2 Variants. *Metabolites* **2023**, *13*, 309. [CrossRef]
10. Hashemian, S.M.R.; Sheida, A.; Taghizadieh, M.; Memar, M.Y.; Hamblin, M.R.; Bannazadeh Baghi, H.; Sadri Nahand, J.; Asemi, Z.; Mirzaei, H. Paxlovid (Nirmatrelvir/Ritonavir): A New Approach to COVID-19 Therapy? *Biomed. Pharmacother.* **2023**, *162*, 114367. [CrossRef]
11. Yang, Z. Elucidation of the Pharmacological Development and Action Mechanism of Remdesivir and Paxlovid in Combatting COVID-19. *MedScien* **2024**, *1*, 1752. [CrossRef]
12. Zhang, Y.-N.; Zhang, Q.-Y.; Li, X.-D.; Xiong, J.; Xiao, S.-Q.; Wang, Z.; Zhang, Z.-R.; Deng, C.-L.; Yang, X.-L.; Wei, H.-P.; et al. Gemcitabine, Lycorine and Oxysophoridine Inhibit Novel Coronavirus (SARS-CoV-2) in Cell Culture. *Emerg. Microbes Infect.* **2020**, *9*, 1170–1173. [CrossRef]
13. Jin, Y.-H.; Min, J.S.; Jeon, S.; Lee, J.; Kim, S.; Park, T.; Park, D.; Jang, M.S.; Park, C.M.; Song, J.H.; et al. Lycorine, a Non-Nucleoside RNA Dependent RNA Polymerase Inhibitor, as Potential Treatment for Emerging Coronavirus Infections. *Phytomedicine* **2021**, *86*, 153440. [CrossRef]
14. Kurt, B. Investigation of The Potential Inhibitor Effects of Lycorine On Sars-Cov-2 Main Protease (Mpro) Using Molecular Dynamics Simulations and MMPBSA. *Int. J. Life Sci. Biotechnol.* **2022**, *5*, 424–435. [CrossRef]
15. Reed, L.J.; Muench, H. A Simple Method of Estimating FIfty Percent Endpoints. *Am. J. Trop. Med. Hyg.* **1938**, *27*, 493–497.
16. Bhoyar, R.C.; Jain, A.; Sehgal, P.; Divakar, M.K.; Sharma, D.; Imran, M.; Jolly, B.; Ranjan, G.; Rophina, M.; Sharma, S.; et al. High Throughput Detection and Genetic Epidemiology of SARS-CoV-2 Using COVIDSeq Next-Generation Sequencing. *PLoS ONE* **2021**, *16*, e0247115. [CrossRef]
17. Katoh, K.; Standley, D.M. MAFFT Multiple Sequence Alignment Software Version 7: Improvements in Performance and Usability. *Mol. Biol. Evol.* **2013**, *30*, 772–780. [CrossRef] [PubMed]
18. Batool, S.; Chokkakula, S.; Jeong, J.H.; Baek, Y.H.; Song, M.-S. SARS-CoV-2 Drug Resistance and Therapeutic Approaches. *Heliyon* **2025**, *11*, e41980. [CrossRef] [PubMed]
19. Lei, J.; Kusov, Y.; Hilgenfeld, R. Nsp3 of Coronaviruses: Structures and Functions of a Large Multi-Domain Protein. *Antivir. Res.* **2018**, *149*, 58–74. [CrossRef]
20. Taha, T.Y.; Suryawanshi, R.K.; Chen, I.P.; Correy, G.J.; McCavitt-Malvido, M.; O'Leary, P.C.; Jogalekar, M.P.; Diolaiti, M.E.; Kimmerly, G.R.; Tsou, C.-L.; et al. A Single Inactivating Amino Acid Change in the SARS-CoV-2 NSP3 Mac1 Domain Attenuates Viral Replication in Vivo. *PLoS Pathog.* **2023**, *19*, e1011614. [CrossRef] [PubMed]
21. Roe, M.K.; Junod, N.A.; Young, A.R.; Beachboard, D.C.; Stobart, C.C. Targeting Novel Structural and Functional Features of Coronavirus Protease Nsp5 (3CLpro, Mpro) in the Age of COVID-19. *J. General. Virol.* **2021**, *102*, 001558. [CrossRef]
22. Iketani, S.; Mohri, H.; Culbertson, B.; Hong, S.J.; Duan, Y.; Luck, M.I.; Annavajhala, M.K.; Guo, Y.; Sheng, Z.; Uhlemann, A.-C.; et al. Multiple Pathways for SARS-CoV-2 Resistance to Nirmatrelvir. *Nature* **2023**, *613*, 558–564. [CrossRef] [PubMed]
23. Jochmans, D.; Liu, C.; Donckers, K.; Stoycheva, A.; Boland, S.; Stevens, S.K.; De Vita, C.; Vanmechelen, B.; Maes, P.; Trüeb, B.; et al. The Substitutions L50F, E166A, and L167F in SARS-CoV-2 3CLpro Are Selected by a Protease Inhibitor In Vitro and Confer Resistance to Nirmatrelvir. *mBio* **2023**, *14*, e02815-22. [CrossRef]
24. Zhou, Y.; Gammeltoft, K.A.; Ryberg, L.A.; Pham, L.V.; Tjørnelund, H.D.; Binderup, A.; Duarte Hernandez, C.R.; Fernandez-Antunez, C.; Offersgaard, A.; Fahnøe, U.; et al. Nirmatrelvir-Resistant SARS-CoV-2 Variants with High Fitness in an Infectious Cell Culture System. *Sci. Adv.* **2022**, *8*, eadd7197. [CrossRef] [PubMed]
25. Lewandowski, E.M.; Zhang, X.; Tan, H.; Jaskolka-Brown, A.; Kohaal, N.; Frazier, A.; Madsen, J.J.; Jacobs, L.M.C.; Wang, J.; Chen, Y. Distal Protein-Protein Interactions Contribute to Nirmatrelvir Resistance. *Nat. Commun.* **2025**, *16*, 1266. [CrossRef]
26. Tahir, M. Coronavirus Genomic nsp14-ExoN, Structure, Role, Mechanism, and Potential Application as a Drug Target. *J. Med. Virol.* **2021**, *93*, 4258–4264. [CrossRef] [PubMed]
27. Hassan, S.S.; Bhattacharya, T.; Nawn, D.; Jha, I.; Basu, P.; Redwan, E.M.; Lundstrom, K.; Barh, D.; Andrade, B.S.; Tambuwala, M.M.; et al. SARS-CoV-2 NSP14 Governs Mutational Instability and Assists in Making New SARS-CoV-2 Variants. *Comput. Biol. Med.* **2024**, *170*, 107899. [CrossRef]

28. Vu, M.N.; Lokugamage, K.G.; Plante, J.A.; Scharton, D.; Bailey, A.O.; Sotcheff, S.; Swetnam, D.M.; Johnson, B.A.; Schindewolf, C.; Alvarado, R.E.; et al. QTQTN Motif Upstream of the Furin-Cleavage Site Plays a Key Role in SARS-CoV-2 Infection and Pathogenesis. *Proc. Natl. Acad. Sci. USA* **2022**, *119*, e2205690119. [CrossRef]
29. Santos-Mendoza, T. The Envelope (E) Protein of SARS-CoV-2 as a Pharmacological Target. *Viruses* **2023**, *15*, 1000. [CrossRef]
30. Schoeman, D.; Fielding, B.C. Is There a Link Between the Pathogenic Human Coronavirus Envelope Protein and Immunopathology? A Review of the Literature. *Front. Microbiol.* **2020**, *11*, 2086. [CrossRef]
31. Arduini, A.; Laprise, F.; Liang, C. SARS-CoV-2 ORF8: A Rapidly Evolving Immune and Viral Modulator in COVID-19. *Viruses* **2023**, *15*, 871. [CrossRef] [PubMed]
32. Li, J.Y.; Liao, C.H.; Wang, Q.; Tan, Y.J.; Luo, R.; Qiu, Y.; Ge, X.Y. The ORF6, ORF8 and Nucleocapsid Proteins of SARS-CoV-2 Inhibit Type I Interferon Signaling Pathway. *Virus Res.* **2020**, *286*, 198074. [CrossRef] [PubMed]
33. Narayanan, K.; Huang, C.; Makino, S. SARS Coronavirus Accessory Proteins. *Virus Res.* **2008**, *133*, 113–121. [CrossRef]
34. Gong, Y.-N.; Tsao, K.-C.; Hsiao, M.-J.; Huang, C.-G.; Huang, P.-W.P.-N.; Huang, P.-W.P.-N.; Lee, K.-M.; Liu, Y.-C.Y.-C.Y.-C.; Yang, S.-L.; Kuo, R.-L.; et al. SARS-CoV-2 Genomic Surveillance in Taiwan Revealed Novel ORF8-Deletion Mutant and Clade Possibly Associated with Infections in Middle East. *Emerg. Microbes Infect.* **2020**, *9*, 1457–1466. [CrossRef] [PubMed]
35. Hassan, S.S.; Kodakandla, V.; Redwan, E.M.; Lundstrom, K.; Choudhury, P.P.; El-Aziz, T.M.A.; Takayama, K.; Kandimalla, R.; Lal, A.; Serrano-Aroca, Á.; et al. An Issue of Concern: Unique Truncated ORF8 Protein Variants of SARS-CoV-2. *PeerJ* **2022**, *10*, e13136. [CrossRef]
36. Mazur-Panasiuk, N.; Rabalski, L.; Gromowski, T.; Nowicki, G.; Kowalski, M.; Wydmanski, W.; Szulc, P.; Kosinski, M.; Gackowska, K.; Drweska-Matelska, N.; et al. Expansion of a SARS-CoV-2 Delta Variant with an 872 Nt Deletion Encompassing ORF7a, ORF7b and ORF8, Poland, July to August 2021. *Euro Surveill. Bull. Eur. Sur Les Mal. Transm. Eur. Commun. Dis. Bull.* **2021**, *26*, 1–6. [CrossRef]
37. Zinzula, L. Lost in Deletion: The Enigmatic ORF8 Protein of SARS-CoV-2. *Biochem. Biophys. Res. Commun.* **2020**, *54*, 251–255. [CrossRef]
38. Wagner, C.; Kistler, K.E.; Perchetti, G.A.; Baker, N.; Frisbie, L.A.; Torres, L.M.; Aragona, F.; Yun, C.; Figgins, M.; Greninger, A.L.; et al. Positive Selection Underlies Repeated Knockout of ORF8 in SARS-CoV-2 Evolution. *Nat. Commun.* **2024**, *15*, 3207. [CrossRef]
39. Sanderson, T.; Hisner, R.; Donovan-Banfield, I.; Hartman, H.; Løchen, A.; Peacock, T.P.; Ruis, C. A Molnupiravir-Associated Mutational Signature in Global SARS-CoV-2 Genomes. *Nature* **2023**, *623*, 594–600. [CrossRef]
40. Strizki, J.; Murgolo, N.; Gaspar, J.; Howe, J.; Hutchins, B.; Mohri, H.; Ho, D.D.; Hazuda, D.; Grobler, J. 153. Molnupiravir Exhibits a High Barrier to the Development of SARS-CoV-2 Resistance in Vitro. *Open Forum Infect. Dis.* **2022**, *9*, ofac492.231. [CrossRef]
41. Gratteri, C.; Ambrosio, F.A.; Lupia, A.; Moraca, F.; Catalanotti, B.; Costa, G.; Bellocchi, M.; Carioti, L.; Salpini, R.; Ceccherini-Silberstein, F.; et al. Molecular and Structural Aspects of Clinically Relevant Mutations of SARS-CoV-2 RNA-Dependent RNA Polymerase in Remdesivir-Treated Patients. *Pharmaceuticals* **2023**, *16*, 1143. [CrossRef]
42. Stevens, L.J.; Pruijssers, A.J.; Lee, H.W.; Gordon, C.J.; Tchesnokov, E.P.; Gribble, J.; George, A.S.; Hughes, T.M.; Lu, X.; Li, J.; et al. Mutations in the SARS-CoV-2 RNA-Dependent RNA Polymerase Confer Resistance to Remdesivir by Distinct Mechanisms. *Sci. Transl. Med.* **2022**, *14*, eabo0718. [CrossRef]
43. Khater, S.; Kumar, P.; Dasgupta, N.; Das, G.; Ray, S.; Prakash, A. Combining SARS-CoV-2 Proofreading Exonuclease and RNA-Dependent RNA Polymerase Inhibitors as a Strategy to Combat COVID-19: A High-Throughput in Silico Screening. *Front. Microbiol.* **2021**, *12*, 647693. [CrossRef] [PubMed]
44. Wang, X.; Sacramento, C.Q.; Jockusch, S.; Chaves, O.A.; Tao, C.; Fintelman-Rodrigues, N.; Chien, M.; Temerozo, J.R.; Li, X.; Kumar, S.; et al. Combination of Antiviral Drugs Inhibits SARS-CoV-2 Polymerase and Exonuclease and Demonstrates COVID-19 Therapeutic Potential in Viral Cell Culture. *Commun. Biol.* **2022**, *5*, 154. [CrossRef] [PubMed]
45. Tamama, K. Potential Benefits of Dietary Seaweeds as Protection Against COVID-19. *Nutr. Rev.* **2021**, *79*, 814–823. [CrossRef]
46. Emeny, J.M.; Morgan, M.J. Regulation of the Interferon System: Evidence That Vero Cells Have a Genetic Defect in Interferon Production. *J. Gen. Virol.* **1979**, *43*, 247–252. [CrossRef]
47. Ogando, N.S.; Dalebout, T.J.; Zevenhoven-Dobbe, J.C.; Limpens, R.W.A.L.; Van Der Meer, Y.; Caly, L.; Druce, J.; De Vries, J.J.C.; Kikkert, M.; Bárcena, M.; et al. SARS-Coronavirus-2 Replication in Vero E6 Cells: Replication Kinetics, Rapid Adaptation and Cytopathology. *J. Gen. Virol.* **2020**, *101*, 925–940. [CrossRef] [PubMed]
48. Jureka, A.S.; Basler, C.F. Propagation and Quantification of SARS-CoV-2. In *SARS-CoV-2*; Chu, J.J.H., Ahidjo, B.A., Mok, C.K., Eds.; Methods in Molecular Biology; Springer: New York, NY, USA, 2022; Volume 2452, pp. 111–129. ISBN 978-1-0716-2110-3.
49. Matsuyama, T.; Kubli, S.P.; Yoshinaga, S.K.; Pfeffer, K.; Mak, T.W. An Aberrant STAT Pathway Is Central to COVID-19. *Cell Death Differ.* **2020**, *27*, 3209–3225. [CrossRef]